

Electrodynamics of Dipolar Beads in an Electrophoretic Spherical Cavity

M.H. Lean and A.R. Völkel

Palo Alto Research Center, Palo Alto, CA 94304, US
 meng.lean@parc.com , armin.volkel@parc.com

Abstract – This paper describes an algorithm to simulate transient behavior of a dipolar bead in an electrophoretic spherical cavity. The model includes consideration of form drag and viscous damping, both corrected for wall effects. In particular, the bead rotation as a function of monopole and dipole charge, and the impact of gravity on the bead dynamics is investigated. Several levels of approximation are implemented to expedite the overall computation. A consistent set of results is presented to describe the accuracy of the simulation.

I. INTRODUCTION

The transient dynamics of dipolar beads in an electrophoretic spherical cavity presents an interesting phenomenon, because it captures the interplay of electrophoretics, particle dynamics, and tribology. The problem geometry is described by a dipolar bead immersed in a polarized fluid within the cavity. Switching bias voltages are applied to induce both translational and rotational motion of the bead. This paper details a model of coupled phenomena which employs ODE's to describe the bead dynamics, integral equations for the field solution, and particle simulation for the bipolar migrations. Special focus is given to the impact of confinement and gravitational force on the bead dynamics.

II. PROBLEM FORMULATION

We assume a dipolar bead with radius r_b and mass m in a spherical cavity of radius r_c . The bead is divided into two distinct hemispheres with different net charges q_b and q_w . For low counter ion concentrations, we can approximate the charge distribution on the bead by the first two terms of a multipole expansion, i.e. by the monopole charge $q_m = q_b + q_w$ and the dipole moment $\mathbf{p} = q_d d_p$, where $q_d = |q_b - q_w|/2$ is the dipole charge and d_p is the distance between the hemispherical charges q_w and q_b . This dipole length d_p depends on the actual distribution of charge on each hemisphere, and is given by $2r_b$, r_b , and $3r_b/4$ for uniform polar, surface, and volume distributions in each hemisphere, respectively.

External electrodes are placed above and below the cavity. Fig. 1 shows a schematic 2D cross section of the computational cell. The cavity is centered between the top and bottom electrode, and all linear dimensions (width W , length L , and height H) are identical for the uniform cube. The whole system is filled with a liquid that exhibits a low, but finite conductivity σ (e.g. we can

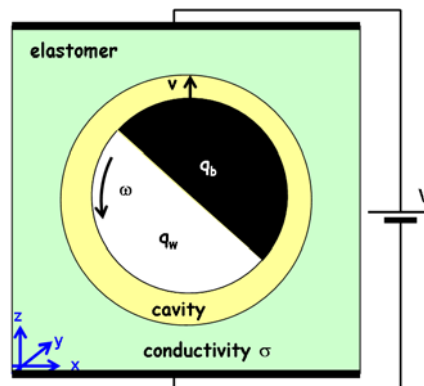


Fig. 1: Cross-section of unit cell with one dipolar bead inside the cavity. Shown dimensions are not to scale. For the present discussion we assume a cavity radius that is 25% larger than the bead radius.

think of the sheet material as a gel that has been swollen with an oil). Fig. 2 shows a snapshot of the animated

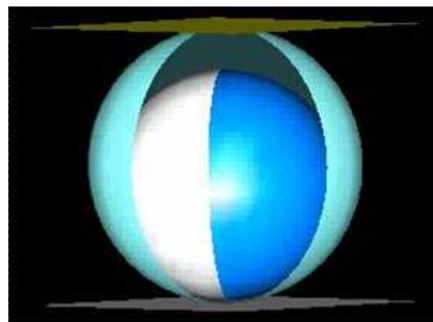


Fig. 2: 3D snapshot of animation of dipolar bead inside the cavity. One quadrant of the cavity wall has been removed for clarity. The graphic is rendered using the commercial software package AVS.

dipolar bead dynamics within a spherical cavity.

A. Translational Motion

The translational motion is governed by Newton's equation

$$m\ddot{\mathbf{R}} = q_m \mathbf{E} + (\mathbf{p} \cdot \nabla) \mathbf{E} - \Gamma_t f_t(\mathbf{R}) \dot{\mathbf{R}} - m_b g \mathbf{e}_z, \quad (1)$$

where Γ_t is the translational drag coefficient, m_b is the buoyant mass of the bead, and g is the gravitational accel-

eration. For beads with a radius of $r_b \approx 50\mu\text{m}$ the gravitational force becomes relevant for the bead dynamics, if the bead and solvent densities are not well matched (i.e. $m_b \neq 0$). The parameter $f_t(\mathbf{R})$ is a position-dependent drag correction due to the cavity walls, and has been chosen as [1]

$$f_t(\mathbf{R}) = 1 + \frac{2\epsilon}{\epsilon^2 - \xi^2}, \quad (2)$$

where $\xi = |\mathbf{R} - \mathbf{r}_c|/r_b$ is the scaled actual distance of the bead center from the cavity center \mathbf{r}_c , while $\epsilon = (r_c - r_b)/r_b$ is the maximal possible distance of the bead center from the cavity center.

The first term on the right-hand-side of Eqn. 1 is the Coulomb force due to the electrostatic field. The second term is a dipole force, which includes both the Clausius-Mossotti contribution and a “hard” dipole due to the assigned hemispherical charges. The third term is the form drag, which is dependent on the shape of the bead and its location relative to the cavity walls. For spherical particles at low speed this term reduces to the Stokes drag $\Gamma_t = 6\pi\eta r_b$ modified by the wall correction factor (Eqn. 2) (η is the viscosity of the fluid inside the cavity). From Eqn. 2 we see that drag increases significantly when the bead is in close proximity to the wall.

B. Rotational Motion

Bead rotation is governed by the torque equation

$$I\dot{\Omega} = \mathbf{p} \times \mathbf{E} - k\Gamma_r f_r(\mathbf{R})\Omega, \quad (3)$$

where Ω is the angular velocity, I is the moment of inertia of the bead, and Γ_r is the rotational drag coefficient. The position dependent parameter f_r describes the wall corrections to the rotational drag and has been chosen as [2]

$$f_r(\mathbf{R}) = 1 + \frac{1}{\epsilon_1} \ln\left(\frac{2\epsilon_1}{\epsilon - \xi}\right), \quad (4)$$

where $\epsilon_1 = \epsilon/(1 + \epsilon)$. The parameter k depends on material and operational properties, and can be chosen to control the oscillation of the bead about its equilibrium position. An estimate for k is given by the particular solution

$$k = \frac{2\sqrt{pEI}}{\Gamma_r} \quad (5)$$

to Eqn. 3, which results in critically damped oscillations of the electrical dipole of the bead around the direction of the applied electric field.

C. Field Solution

Several levels of approximations are implemented to expedite computations. The most accurate version solves

for the electrostatic field using a boundary integral equation method [3] that takes into account contributions from the diverse collection of free charge, interfacial bound charge, volume space charge, and assigned bead charge. Lower order versions may be invoked through combinations of image symmetries, analytic representations, particle-particle mesh (PPPM) scheme [4], and “super-ion” or particle clumping [5] schemes.

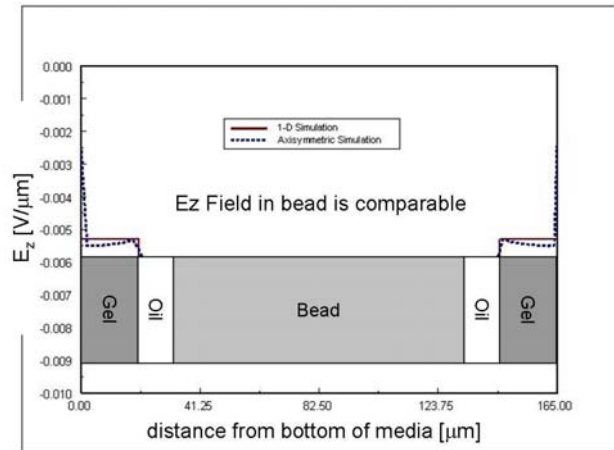


Fig. 3: Explicit electric field calculation along a straight line through the center of a bead in the model system. Since the dielectric constants of the different materials are very similar, the electric field changes only very slightly within the sheet.

Fig. 3 shows the electric field due to an applied bias voltage calculated along a line through the center of the bead using a 1D and a cylindrical symmetric model. Both models give very similar results, with the axisymmetric model exhibiting departure from 1D fields near the polar regions of the bead and the cavity due to the finite curvature of the interface regions.

D. Time Integration Algorithm

Difference formulas are used for time integration of the second order differential equations. The central difference approximation

$$\ddot{\mathbf{R}} = \frac{[\mathbf{R}(t + \Delta t) - 2\mathbf{R}(t) + \mathbf{R}(t - \Delta t)]}{\Delta t^2} \quad (6)$$

may be rearranged to result in

$$\mathbf{R}(t_+) = 2\mathbf{R}(t) - \mathbf{R}(t_-) + \frac{\mathbf{F}(t) - \mathbf{F}_{drag}}{m\Delta t^2} \quad (7a)$$

$$\Theta(t_+) = 2\Theta(t) - \Theta(t_-) + \frac{\mathbf{T}_\Theta(t) - \mathbf{T}_{\Theta,drag}}{I\Delta t^2}, \quad (7b)$$

$$\Psi(t_+) = 2\Psi(t) - \Psi(t_-) + \frac{\mathbf{T}_\Psi(t) - \mathbf{T}_{\Psi,drag}}{I\Delta t^2}, \quad (7c)$$

where Eqn. 7a represents the three cartesian coordinates of the bead position, Eqns. 7b and 7c represent the corresponding torque equations resolved in the two independent spherical angles, and $t_{\pm} = t \pm \Delta t$.

E. Boundary Conditions

Since charge-charge interactions are long-range, we have to choose proper boundary conditions to avoid non-physical behavior in our finite-size computational cell.

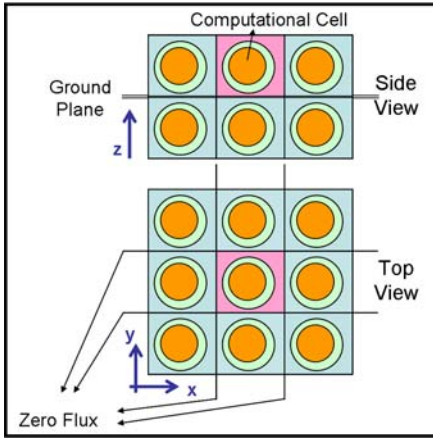


Fig. 4: Schematic drawing of image cells used to implement the different boundary conditions.

In order to satisfy the ground plane boundary condition at the bottom of the sheet ($z = 0$), a mirror image with opposite charge for each ion has to be considered (Fig. 4, top).

For zero-flux boundary condition we have to satisfy the condition $\mathbf{E}_n = 0$ on each of the vertical sidewalls, where \mathbf{E}_n is the normal component of the electric field on the boundary. This can be approximated by placing mirror-symmetric nearest neighbor image cells in the xy plane (Fig. 4, bottom). More accurate approximations would include more terms (mirror image cells) in this series expansion.

If we want to allow ions to move in and out of the computational cell, one can impose periodic boundary conditions on the vertical sidewalls, where ions moving out of one side wall re-enter from the opposite sidewall. These can be achieved by placing nearest neighbor image cells with the identical ion distribution as in the computational cell in the xy plane.

III. RESULTS AND DISCUSSION

Both, Eqn. 1 and Eqn. 3, can be made dimensionless by introducing proper length and time scales. In the case of bead translation it is convenient to introduce as length

scale the bead radius r_b and as time scale $\tau_t = m/\Gamma_t$, which leads to the dimensionless equation of motion

$$\ddot{\xi} = \tau b - f_t(\xi)\dot{\xi} \quad (8)$$

with

$$b = \frac{q_m E - m_b g}{\Gamma_t r_b}. \quad (9)$$

Note that the time scale here measures the time over which inertial effects dominate over drag effects. At times $t \gg \tau_t$ we can ignore the inertial term. In this case Eqn. 8 has the analytic solution

$$bt = \xi + \xi_0 + 2[\text{arctgh}(\xi/\epsilon) + \text{arctgh}(\xi_0/\epsilon)], \quad (10)$$

where t is the real system time (i.e. we now have the drag dominated time scale $\tau = 1/|b|$), and ξ_0 is the position of the bead at $t = 0$. Because the drag correction diverges as the distance of the bead from the cavity wall goes to zero, it also takes a very long time for the bead to touch the cavity wall. In computer simulations we therefore limit the bead translation such that each bead always keeps a minimum distance from the cavity wall to prevent numerical divergences. The additional rationale is that surface roughness would result in this order of magnitude spacing between the bead and cavity surfaces.

The sign of the parameter b determines whether the bead moves up ($b > 0$) or down ($b < 0$). The gravitational force breaks the symmetry between up and down translation times for a fixed applied voltage. In particular, the bead can travel upward only, if the electric field is strong enough to overcome gravity, i.e.

$$q_m E > m_b g. \quad (11)$$

Fig. 5 shows the minimal monopole charge q_m required for a given bead size and applied voltage. For a bead with $r_b = 45\mu m$, $q_m = 8fC$, and $m_b = 0.29 * m_{bead}$, a field of at least $E \geq 0.16V/\mu m$ is required before it moves against gravity.

The bead rotation is characterized by the time scale $\tau_r = \sqrt{I/pE}$ and the dimensionless version of Eqn. 7b becomes

$$\ddot{\Theta} = \sin \Theta - 2f_r(\xi)\dot{\Theta}. \quad (12)$$

In the case where the inertial term can be neglected in the equation of motion for the bead rotation the dipole orientation angle is given by the closed form

$$\Theta(\hat{t}) = 2 \arctg \left\{ \exp \left[\int \frac{d\hat{t}}{2f_r(\xi(\hat{t}))} \right] \right\}, \quad (13)$$

where $\hat{t} = t/\tau_r$ is the dimensionless time parameter.

Without the wall correction to the rotational drag ($f_r = 1$) the bead rotation is completely specified by its size and shape (which determine the moment of inertia I), its dipole moment p , and the applied electric

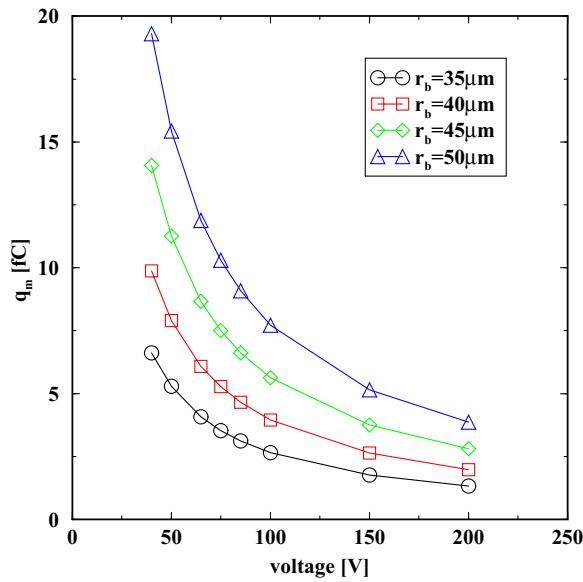


Fig. 5: Minimal monopole charge required to levitate a bead of radius r_b for a given applied voltage assuming a sheet thickness $H = 450\mu\text{m}$.

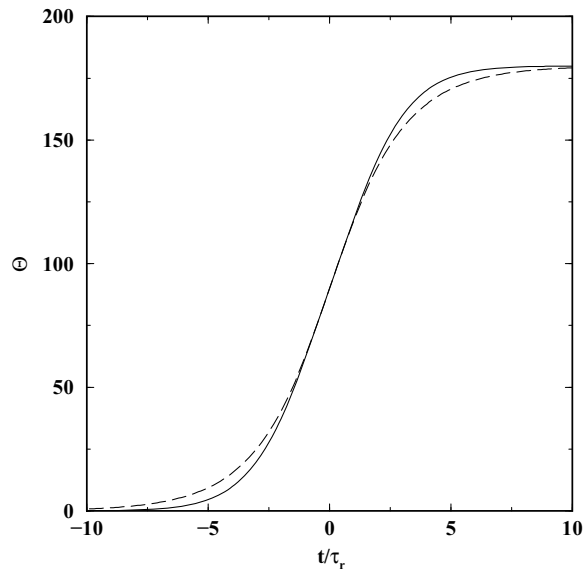


Fig. 6: Bead orientation as function of scaled time for a system without wall drag corrections. (solid): complete solution of Eqn. 12; (dashed): solution of Eqn. 12 without the inertial term $\ddot{\Theta}$.

field. Fig. 6 shows the bead orientation as a function of dimensionless time for this case. The inertial term of Eqn. 12 has the most effect when the bead dipole is closely aligned with the electric field, where it slows down the bead rotation visibly. Without the inertial term, the

bead rotation is described by the function

$$\Theta(\hat{t}) = 2 \arctg \left\{ \exp \left[\frac{\hat{t} - \hat{t}_0}{2} \right] \right\}, \quad (14)$$

where \hat{t}_0 is the time at which $\Theta = \pi/2$.

With the wall drag fully included the translational and rotational equation of motion become coupled and a numerical approach is needed to solve for the bead dynamics.

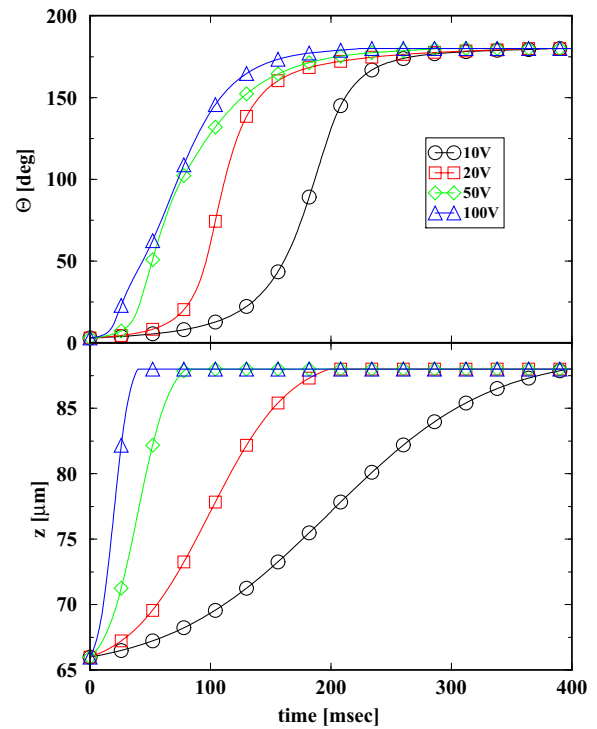


Fig. 7: Bead orientation angle and position as function of time for different applied voltages and zero buoyant mass ($m_b = 0$).

Fig. 7 shows typical orientation and position curves as function of time for a bead moving inside the cavity. In the case when the density of the bead material is matched by the density of the solvent, the buoyant mass m_b is zero and the response of the bead becomes independent on the direction of the applied field. However, because of the coupling between the translational and translational dynamics through the drag coefficients, we observe quite different rotation speeds as function of applied field: For free rotation, we would expect a rotation time scale that is inversely proportional to the square root of the applied field. With the impact of the walls on the drag, we observe instead a slowing down of the bead rotation times at increased applied voltage (50V and 100V in Fig. 7). This is due to the fact that at these voltages the bead moves through the cavity before it has a chance to rotate, so most of its orientation change happens near the cavity wall where the drag is highest.

When the buoyant mass of the bead is not zero, the bead is also influenced by gravity, and its response to an applied electric field depends on the orientation of this field to the gravitational field. Fig. 8 shows bead

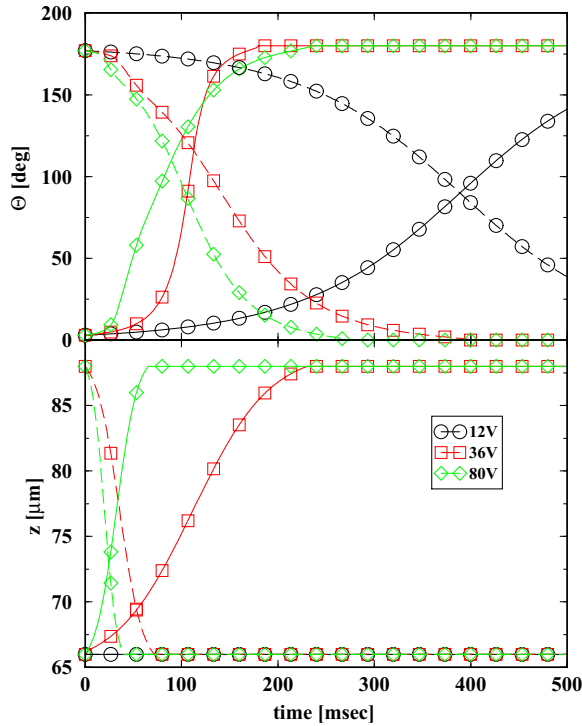


Fig. 8: Bead orientation angle and position as function of time for different applied voltages and buoyant mass $m_b = 0.29m_{bead}$. (solid line): upward motion; (dashed line): downward motion.

orientation and position as function of time for a bead with buoyant mass $m_b = 0.29 * m_{bead}$ for different applied fields that are either parallel or anti-parallel to gravity, causing the bead to either move up or down. Again, we see that the biggest impact on the rotation time scale of the bead is its location relative to the cavity wall. In particular, we observe, that for the case when the field is parallel to gravity (bead moves down) the translational motion is much faster than the rotational motion, and the bead always changes its orientation close to the bottom of the cavity. Also, because of its finite buoyant mass the bead does not move upward for low applied voltages (10V case in Fig. 8).

In order to discuss the rotation times for beads with different monopole and dipole charges and buoyant masses, we fitted the time-dependent orientation change to a standard step function. In particular, we fitted the expression

$$F(t) = \sin^2\left(\frac{\Theta(t)}{2}\right) \quad (15)$$

to the ‘‘Fermi-like’’ function

$$R_{fit}(t) = \frac{1}{1 + \exp((t - t_0)/\tau_r)}, \quad (16)$$

with the two fit parameters τ_r , which represents the time scale of rotation, and t_0 , which denotes the time when the bead rotates through $\Theta = 90^\circ$. The expression $F(t)$ corresponds to the projection of the visible part of one hemisphere onto a plane perpendicular to the applied field. The fit function Eqn. 16 is motivated by the solution to the freely rotating sphere without wall drag correction (Eqn. 14). Though this function is expected to represent

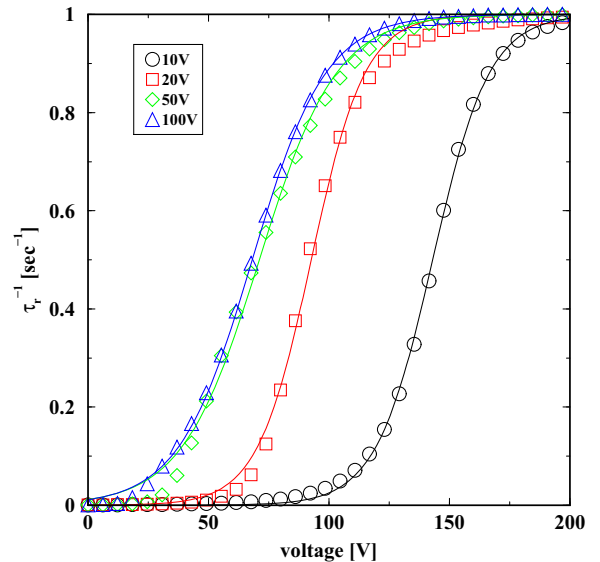


Fig. 9: Fits of time-dependence of bead orientation to Eqn. 8.

a good description of the bead rotation only, when the bead rotates without changing position within the cavity, we observe that it captures the main orientation change very well in all situations encountered by our simulations, as is demonstrated in Fig. 9. In all cases shown, the function fits the steepest part of the rotation curve very well, while it may deviate from the observed data at small and large orientation angles.

Figs. 10, 11, and 12 show fitted rotation times as function of applied voltage for beads with different buoyant mass, monopole charge, and dipole charge, respectively.

At zero buoyant mass the bead translation and rotation times are independent of the applied field, but are shortest for the applied voltage where the rotation takes place while the bead moves through the center of the cavity (at about 20V for the situation shown in Fig. 10). For smaller or larger voltages, the bead rotates closer to the cavity wall and the rotation times are substantially longer. For high applied voltages the bead moves across the cavity before it has a chance to rotate, and the observed inverse rotation times again decrease with voltage as we expect for the case where the bead rotates

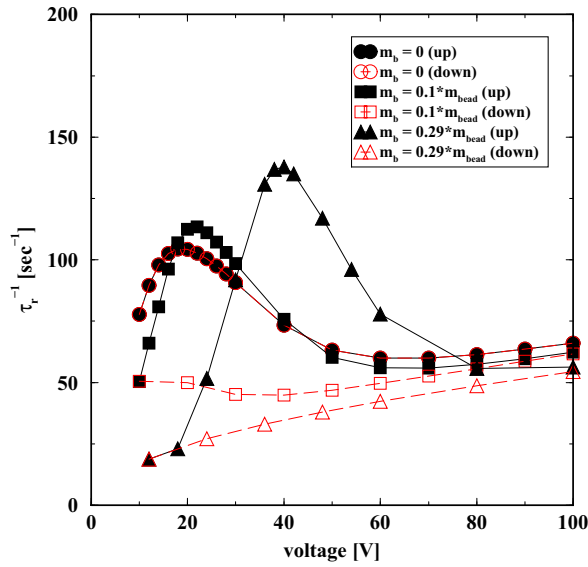


Fig. 10: Inverse bead orientation times as function of applied voltage for different buoyant masses m_b . (solid line): upward motion; (dashed line): downward motion.

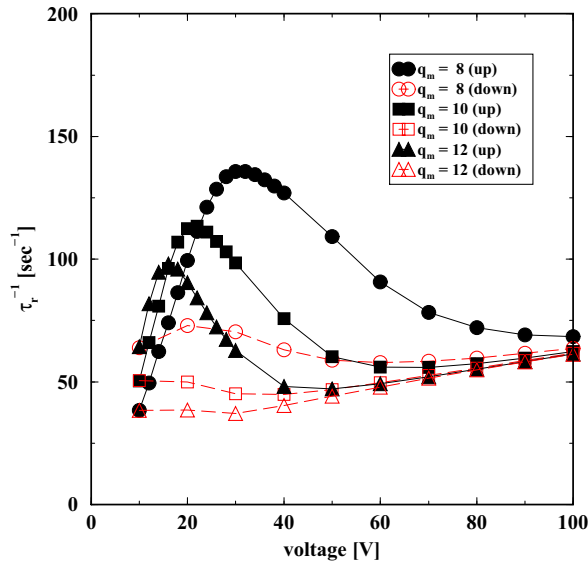


Fig. 11: Inverse bead orientation times as function of applied voltage for different bead monopole charge q_m [in fC], but constant dipole charge $q_d = 4fC$. (solid line): upward motion; (dashed line): downward motion.

at a fixed location within the cavity. For beads with a finite buoyant mass, gravity either speeds up or slows down the translational motion, and the rotation times become dependent on the direction of the applied field. In particular, for the case where the field moves the bead downward, translational motion becomes even for small buoyant mass much faster than rotational motion and the bead almost always rotates near the bottom of the

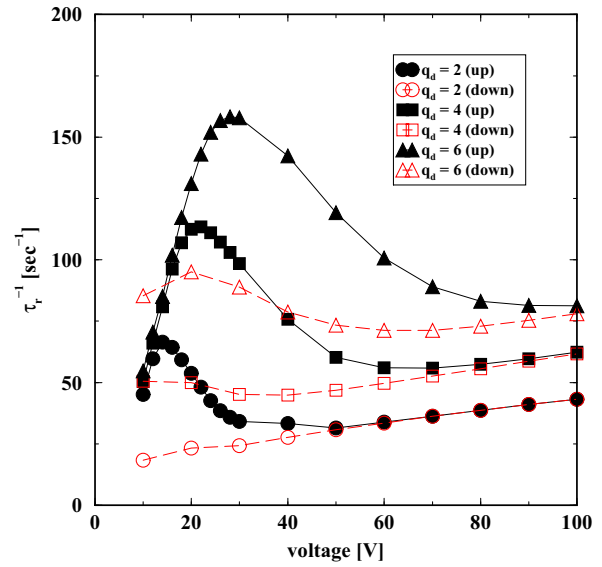


Fig. 12: Inverse bead orientation times as function of applied voltage for different bead dipole charge q_d [in fC], but constant monopole charge $q_m = 10fC$. (solid line): upward motion; (dashed line): downward motion.

cavity.

A change in monopole charge of the bead has the biggest impact on the translational speed of the bead. However, with the coupling of the bead location into the rotational drag, we observe also an impact of varying q_m on the rotational motion, especially at applied voltages where the bead rotation happens near the cavity center (Fig. 11). In particular, we see shorter rotation times for beads with smaller q_m at lower applied voltages when moving downward, and at higher voltages when the bead moves upward.

A change in dipole charge has a direct impact on the rotational speed. In the case where the bead moves downward and rotation happens mainly near the cavity bottom the change in rotation speed is directly related to the dipole moment and we see a linear increase in the inverse rotation time with dipole moment (Fig. 12). For the upward motion we see a shift (increase) in the voltage for which the rotation time is minimal with increasing dipole moment, reflecting the fact that at a higher dipole moment the faster bead rotation requires a slightly faster translational motion to make the bead rotate near the center of the cavity.

An application may be flexible displays, where these dipolar beads are dispersed in an elastomer sheet. Array addressable electrodes on either side of the sheet will allow for controlled switching of the beads to display images.

Fig. 13 shows a comparison of our model to experimental data. Dipolar beads of size $r_b \approx 50\mu m$ have been densely packed into a thin gel matrix that has been swollen with a silicone oil (see e.g. Sheridan et al. [6])

medium such as the solvent), then their main contribution on the bead dynamics will consist of the shielding of the electric field that the bead sees. In particular, if the concentration of these ions is large enough, the electric field at the bead position can become completely shielded (see Fig. 15).

However, if the concentration of the additional charges is small enough to not incur complete shielding of the applied field, the bead will still respond to the external field. Moreover, if the mobility of these charges is reduced, e.g. when moving through the elastomer layer outside of the cavity, the time for those charges to move a distance comparable to the bead size may become of the order of the bead translation and rotation times, leading to competing effects on the bead dynamics. A detailed study of such scenarios will be presented elsewhere.

IV. SUMMARY

This paper described an effective algorithm to simulate the dynamics of a dipolar bead inside a spherical cavity under the influence of an electrostatic field and gravity, subject to wall effects on drag and viscous damping. Using this model we have shown that the wall effects on the drag effectively couple the translational and rotational motion of the bead, leading to a rather rich response behavior of the bead as a function of applied field, bead monopole and bead dipole charge. In addition, if the bead density is not matched exactly by the solvent density, gravity breaks the symmetry between upward and downward motion, which can lead to substantially lower switching times for upward motion due to different locations at which the bead rotates. Several levels of approximation have been implemented to expedite computations, and the accuracy of the model has been verified by analytic solutions. Comparison of our model to dynamic reflectivity measurements on dipolar beads packed into a swollen, low-conductivity, gel matrix show very good agreement at higher applied fields, where the dynamic effects of other mobile charges (e.g. counterions) becomes negligible.

REFERENCES

- [1] H. Brenner, "The slow motion of a sphere through a viscous fluid towards a plane surface", *Chemical Engineering Science*, vol. 16, pp. 242-251, 1961.
- [2] M. Cooley, "The slow rotation in a viscous fluid of a sphere close to another fixed sphere about a diameter perpendicular to the line of centers", *Q. J. Mechanics Appl. Math.*, vol. 24, pp. 237-250, 1971.

- [3] M. H. Lean, "Application of boundary integral equation methods to electromagnetics", *IEEE Trans. Mag.*, vol. 21, pp. 1823-1828, 1985.
- [4] M. H. Lean, "Particle simulations of ion cloud in a magnetic field", *IEEE Trans. Mag.*, vol. 34, pp. 3122-3125, 1998.
- [5] M. H. Lean, J. F. O'Brien, K. Pietrowski, H. Okuda, "Microscopic particle simulation of air ionization", *Proc. NIP-15*, pp. 513-516, 1999.
- [6] N. K. Sheridan, M. A. Berkovitz, "The Gyricon - a twisting ball display", *Proc. S.I.D.*, vol. 18, pp. 289-293, 1977.



Meng H. Lean has 25 years of R&D experience developing multi-physics models from first principles and building hardware prototypes for xerographic and digital imaging applications. He extended the use of boundary element methods in electromagnetics to transient and non-linear couple thermal and fluid dynamic problems. As an adjunct professor at Cornell (1988-1992), he led the implementation of a computational platform for hierarchical simulation of a xerographic color print engine. He has extensive experience in high performance computing in collaboration with researchers at LANL and PPPL. His recent work is in the simulation and development of Bio MEMS devices for bio defense and bio medical applications. Some examples include high-speed high resolution protein separation, bio concentration and enrichment cells, and portable non-contacting surface spore collectors.



Armin R. Völkel received his diploma and Ph.D., both in physics, from the University of Bayreuth, Germany, in 1989 and 1992, respectively. During his graduate studies he was also a Research Assistant at the Los Alamos National Laboratory from 1989 to 1990. He was a postdoc for 6 months at the University of Florence before joining Xerox in 1993, where he worked both at the Xerox Research Center in Canada and, since 2000, at the Palo Alto Research Center. His research interests are in modeling and simulation of complex physical systems including the dynamics of charged particles and polymers in free flow and restricted media under the influence of external electric fields, protein stability, and micro electromechanical systems.